Ultraviolet Photofragmentation Spectroscopy of Alkaline Earth Dication Complexes with Pyridine and 4-Picoline (4-Methyl pyridine)

ARTICLE *in* THE JOURNAL OF PHYSICAL CHEMISTRY A · JUNE 2011

Impact Factor: 2.69 · DOI: 10.1021/jp112171j · Source: PubMed

8 AUTHORS, INCLUDING:

Guohua Wu
University of Nottingham
26 PUBLICATIONS **206** CITATIONS
SEE PROFILE

Lifu Ma
University of Nottingham
9 PUBLICATIONS **35** CITATIONS
SEE PROFILE

Hazel Cox
University of Sussex
38 PUBLICATIONS **521** CITATIONS
SEE PROFILE

THE JOURNAL OF PHYSICAL CHEMISTRY A

ARTICLE

pubs.acs.org/JPCA

Ultraviolet Photofragmentation Spectroscopy of Alkaline Earth Dication Complexes with Pyridine and 4-Picoline (4-Methyl pyridine)

Hamish Stewart,[†] Guohua Wu,[†,§] Lifu Ma,[†] Michael Barclay,[‡] Andreia Dias Vieira,[‡] Andrew King,[‡] Hazel Cox,[*,‡] and Anthony J. Stace[*,†]

[†]Department of Physical and Theoretical Chemistry, School of Chemistry, University of Nottingham, University Park, Nottingham NG7 2RD, United Kindom

[‡]Department of Chemistry and Biochemistry, University of Sussex, Falmer, Brighton BN1 9QJ, United Kingdom

Supporting Information

ABSTRACT: A detailed experimental and theoretical study has been undertaken of the UV photofragmentation spectroscopy of the alkaline earth metal dications Mg^{2+}, Ca^{2+}, and Sr^{2+} complexed with pyridine and 4-methyl pyridine (4-picoline). The ion complexes have been prepared using the pick-up technique and held in an ion trap where their internal temperature has been reduced to <150 K. Exposure of the trapped ions to tunable UV laser radiation leads to the appearance of photofragments with intensities that show significant variation as a function of wavelength. For all three metal dications, the resultant spectra show evidence of resolved features. Time-dependent density functional theory (TDDFT) has been used to identify possible electronic transitions that might be present in the $[M(pyridine)_4]^{2+}$ complexes (M = Mg, Ca, and Sr) within the wavelength range studied. These calculations show that the spectra are dominated by strong $\pi^* \leftarrow \pi$ and weaker $\pi^* \leftarrow$ n transitions localized on the pyridine ligands. The calculations correctly identify those regions of the experimental spectra where UV transitions begin to occur in the complexes and also the wavelengths at which absorption maxima are reached; however, more subtle features of the spectra are difficult to assign with confidence.

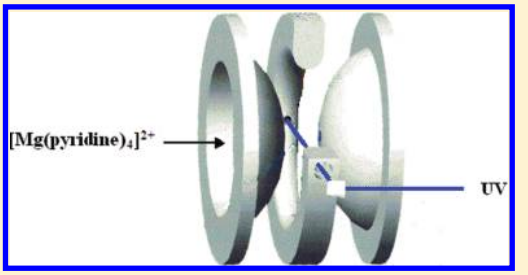

INTRODUCTION

Metal complexes are routinely studied by ultraviolet and visible spectroscopy within solution or in a solid matrix,[1] where inhomogenous broadening and the perturbation of spectra by a solvent and the presence of a counterion are common problems. In contrast, gas-phase spectroscopy has the advantage of allowing the study of isolated species independent of both solvent and counterion, and indeed for singly charged metal complexes a large catalogue of studies now exists at both infrared and UV/visible wavelengths.[2−4] When sufficient number densities can be generated, metal complexes can be studied via photodissociation/photodepletion methods using either infrared multiphoton excitation to generate vibrational spectra or single photon visible/UV excitation to give electronic spectra. However, the overwhelming majority of these gas-phase studies have focused on singly charged ions;[2−4] in contrast, dication metal complexes, while not without examples[5−21] have received far less attention. This observation differs markedly from the circumstances that prevail in nature, where +2 is the most common charge state found for metal ions.[1]

Techniques for the generation and study of stable multiply charged metal complexes in the gas phase have seen significant advances in recent years, making it possible to study a wide range of metals and charge states.[8] Two methods have been used to generate metal dication complexes, and these are electrospray and the pick-up technique.[8] A number of groups have had significant success using electrospray in conjunction with various trapping methods to record both vibrational and electronic spectra.[5,6,11,13−16,18−20] Many of these have involved closed-shell ions; therefore, photoexcitation/depletion has relied on the presence of active modes in the ligands. Evidence of possible ligand field spectra in open-shell transition-metal complexes has come from the electrospray experiments of Spence et al.[5] and Thompson et al.[6] and from a series of pick-up experiments, mainly with a range of Cu^{2+} and Ag^{2+} complexes, where absorption cross sections and low-resolution spectra at visible wavelengths were recorded by Stace et al.[7,9,10] For Ag^{2+} complexes, it was possible to identify through their spectroscopy a reason for the underlying instability of the Ag(II) charge state in condensed phase chemistry.[10] In a recent development in experimental technique, the pick-up method has been combined with a cold ion trap mass spectrometer to yield state-resolved UV photofragmentation spectra of the complexes $[Zn(pyridine)_4]^{2+}$[12] and $[Mn(pyridine)_4]^{2+}$.[17] In the case of $[Zn(pyridine)_4]^{2+}$, it has been possible to combine experimental

Special Issue: A: J. Peter Toennies Festschrift

Received: December 22, 2010
Revised: April 27, 2011
Published: May 13, 2011

and theoretical data for an assignment of the observed transitions as predominantly ligand-based $\pi^* \leftarrow \pi$ and $\pi^* \leftarrow \sigma$ transitions.[12] However, the results also showed that despite having a d^{10} closed-shell electron configuration, orbitals from Zn^{2+} appeared to participate in metal/ligand to ligand charge transfer transitions.[12] A similar combined theoretical and experimental study of $[Mn(pyridine)_4]^{2+}$ was far less conclusive in the assignment of spectroscopic transitions.[17] Although there was evidence of intraligand $\pi^* \leftarrow \pi$ and $\pi^* \leftarrow \sigma$ transitions, a quantitative assignment of metal-based transitions was not possible.[17] In part, the high density of transitions prevented their individual assignment by TDDFT theory, but there are also inherent problems in modeling electronic transitions in a d^5 complex with a single-excitation theory.[21] However, there were spectroscopic features that were common to both Mn^{2+} and Zn^{2+} complexes, and these helped toward a partial identification of electronic transitions.[17]

The significance of UV measurements of the spectra of metal dication complexes is two-fold. First, there is a need to benchmark theoretical methods. Many metal cations, such as Mg^{2+}, Ca^{2+}, and Zn^{2+}, have active biochemical roles,[22,23] and whereas IR spectra may be sensitive to structure, the involvement of a metal ion in chemistry requires an understanding of electronic energy levels. For at least two metal dication complexes, it has been possible to record electronic energy level differences to within 1000 cm^{-1},[12,17] which theory needs to be able to reproduce if it is to be used with confidence in the calculation of chemical pathways. A recent spectroscopic study of $[Mn(pyridine)_4]^{2+}$ revealed serious limitations in the theoretical method.[17] A second requirement for UV spectra on closed-shell metal ions is in the development of spectroscopic markers where the influence an ion has on electronic transitions in a ligand needs to be understood if improvements are to be made in sensitivity and specificity.[24]

In this Article, the results are presented of a combined experimental and theoretical study of the UV spectroscopy of a series of alkaline-earth metal complexes: $[Mg(L)_4]^{2+}$, $[Ca(L)_4]^{2+}$, and $[Sr(L)_4]^{2+}$, where L is either pyridine or 4-methyl pyridine (4-picoline). Pyridine is probably one of the simplest ligands that can be attached to an ion and display some of the characteristics expected of a molecule of biological interest. These characteristics would include metal coordination through a nitrogen atom (e.g., Mg^{2+} in chlorophyll[23]) and the presence of $\pi^* \leftarrow$ n and $\pi^* \leftarrow \pi$ electronic transitions as possible spectroscopic markers. In a previous low-resolution study of the visible spectra of pyridine and 4-methyl pyridine in association with Ag^{2+}, no discernible difference in wavelength dependence was observed.[10] It was anticipated that a study of those regions of their UV spectra where the ligands are spectroscopically active might reveal intraligand transitions but that the closed shell d^0 nature of Group II metal dications would minimize the involvement of their electrons to yield comparatively simple spectra for assignment and elucidation. The contrary example of dissimilar, but still closed-shell, d^{10} Zn^{2+} serves as a reminder that this might not necessarily be the case, particularly for the larger strontium dication. A number of alkaline earth metal dication complexes have already been the subject of spectroscopic studies at both infrared and UV wavelengths.[11,13−16,18−20] Possibly, most relevant to the discussion here is the recent work of Choi et al.[20], who have recorded UV photodepletion spectra from a crown ether complexed with Mg^{2+}, Ca^{2+}, Sr^{2+}, and Ba^{2+}. As a function of increasing cation size, these authors observed a red shift in their spectra, which they attributed to a gradual decrease in the binding energy of the metal ion in the first electronic excited state. Given the significance of calcium in biological systems, it is somewhat surprising that gas-phase complexes of Ca^{2+} have received only limited spectroscopic study;[11,13−16,18−20] however, there have also been studies of quite large Ca^{2+}-containing complexes via collision-induced dissociation.[25−27] Singly charged Ca^+ has been the subject of a quite intensive study, where the isolated 4s valence electron can provide convenient electronic transitions at accessible wavelengths.[2,28,29] Because both magnesium and calcium are biologically important metals,[22,23] studies of their spectra in different ligand environments provide an opportunity to identify the different geometries complexes may adopt and also to explore the possibility of developing spectroscopic markers for the metal ions.

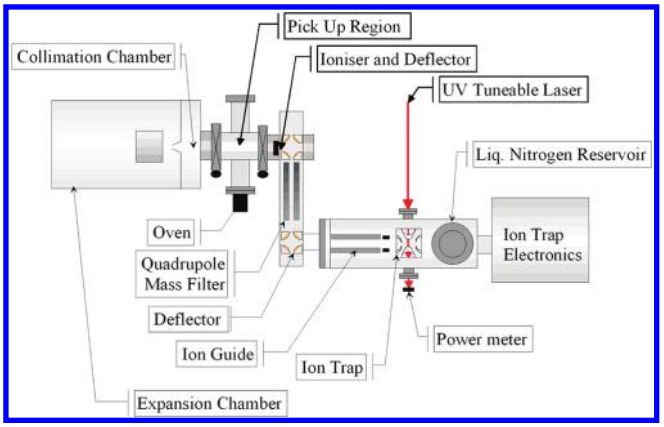

Figure 1. Schematic diagram of the apparatus showing the relative positions of the pick-up source, the quadrupole filter mass, the ion guide, and the quadrupole ion trap.

EXPERIMENTAL SECTION

A schematic diagram of the apparatus is given in Figure 1, and a very detailed description of how it performs has been given elsewhere.[30] In brief, neutral metal−ligand clusters were generated by the pick-up technique.[8] Argon carrier gas at 130 psi was passed through a reservoir to produce a mixture containing ~1% pyridine vapor, which then underwent supersonic expansion through a 50 μm diameter pinhole. After passing through a 1 mm diameter skimmer, the molecular beam containing a mixture of argon and pyridine clusters passed through an atmosphere of metal vapor generated by a Knudson effusion cell. The cell was loaded with chips of the relevant metal and heated to a temperature sufficient to generate a vapor pressure of 10^{-2} to 10^{-3} mbar. Collisions between the vaporized metal atoms and mixed clusters resulted in the "pick up" of metal atoms and the formation of neutral metal−pyridine complexes, which were then ionized by the impact of 100 eV electrons in the ion source of an Extrel quadrupole mass spectrometer.

Each of the $[M(L)_4]^{2+}$ ions were mass-selected and injected into a Paul ion trap, whose end-caps were constantly cooled by a flow of liquid nitrogen from an external reservoir. Collisions with a cold helium buffer gas ($\sim 5 \times 10^{-4}$ mbar) led to a reduction of the internal energy of the ions[30] from 400−500 K to 100−150 K over a 1 s trapping period. In previous experiments, this cooling process has resulted in the emergence of discrete spectroscopic structure[12,17] and represents a significant improvement in resolution when compared with some of the previous examples of

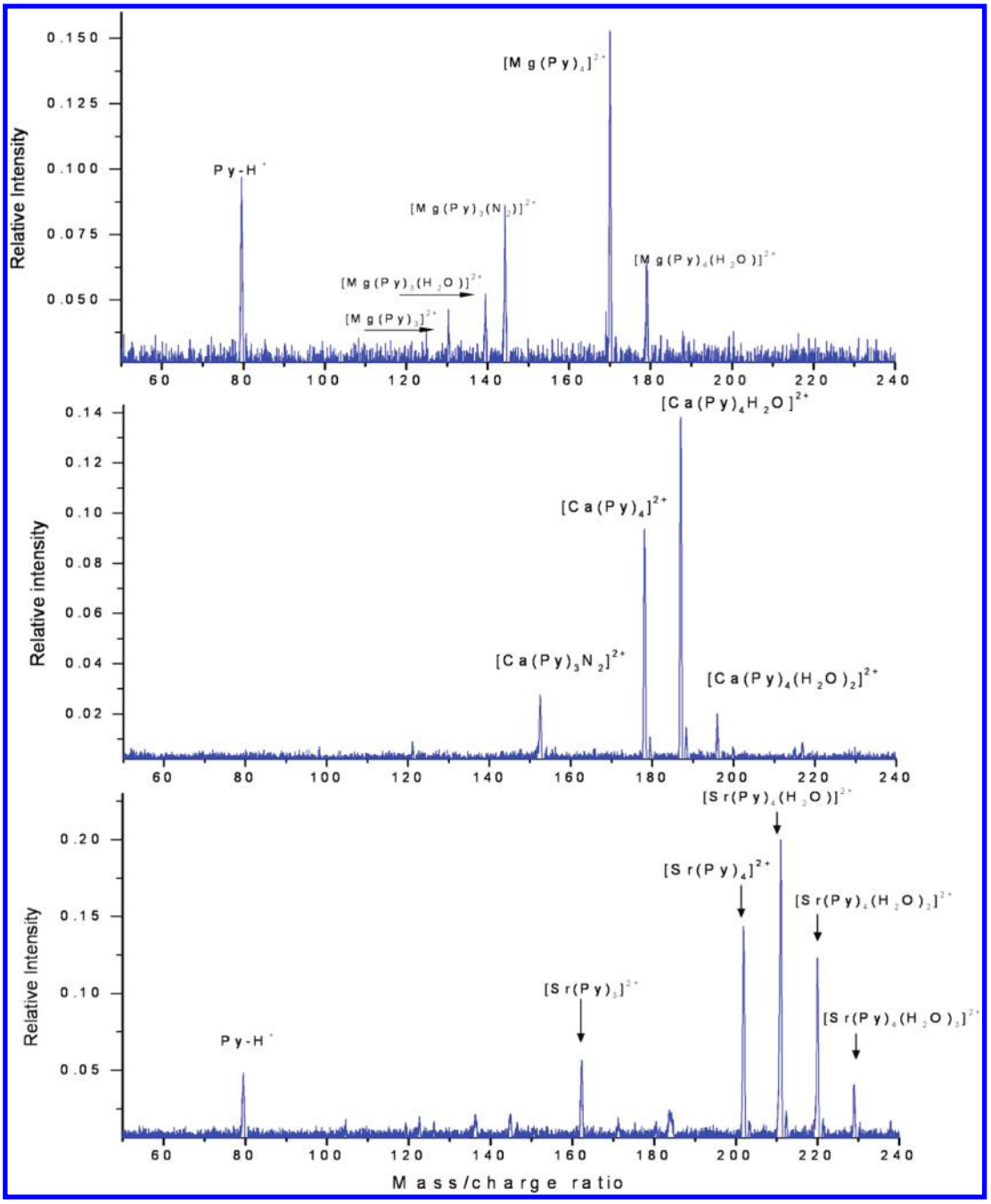

Figure 2. Examples of photofragment mass spectra recorded for each of the Group II metal complexes studied.

metal dication spectra we have recorded.[7,9,10] Because our cooling system envelopes the end-caps of the trap, it is probable that we achieve a lower ion temperature than the ~150 K recorded by Choi et al. using a coldfinger attached to a liquid nitrogen reservoir.[20]

Within a duty cycle of 1 s for ion injection and excitation, 300 ms was devoted to ion collection and cooling before the trapped ions were irradiated with seven 10 ns laser pulses from a frequency-doubled, Nd:YAG pumped dye laser. Precursor ions and any accompanying photofragments were then ejected in the direction of a channeltron detector by ramping the RF voltage on the central electrode of the trap. In this way, each duty cycle generated a complete mass spectrum, which meant that the intensities of all ions could be monitored simultaneously. As a function of laser wavelength, individual mass spectra were collected after averaging ion signals over 200 trap duty cycles. The most frequent fragmentation pathway observed following photon absorption was the loss of a single neutral ligand molecule.

Typical examples of photofragment mass spectra are given for each metal−pyridine complex in Figure 2 and the intensities of the precursor and fragment ions from mass spectra, such as these, were monitored simultaneously to record a photofragment yield at each step in UV wavelength. In common with the previous studies of $[Zn(pyridine)_4]^{2+}$[12] and $[Mn(pyridine)_4]^{2+}$,[17] the injected precursor ions were observed to associate with water

dx.doi.org/10.1021/jp112171j |J. Phys. Chem. A 2011, 115, 6948–6960

Table 1. Comparison between Calculated Transition Energies for Allowed Singlet States of Pyridine and Experiment Data Taken from Gas-Phase UV Spectra[45,47]

		experiment		calculated[a]		
state	type	E^b	f^c	E^b	f^c	contributing transitions
1^1B_1	$\pi^* \leftarrow n$	37 021	0.003	36 852	0.003	$3b_1(\pi^*) \leftarrow 11a_1(n)$ (99%)
1^1B_2	$\pi^* \leftarrow \pi$	40 247	0.029	42 883	0.033	$3b_1(\pi^*) \leftarrow 1a_2(\pi)$ (73%) $2a_2(\pi^*) \leftarrow 2b_1(\pi)$ (26%)
2^1A_1	$\pi^* \leftarrow \pi$	51 458	0.085	50 134	0.013	$2a_2(\pi^*) \leftarrow 1a_2(\pi)$ (61%) $3b_1(\pi^*) \leftarrow 2b_1(\pi)$ (36%)
3^1A_1	$\pi^* \leftarrow \pi$	58 233	0.9	58 467	0.503	$3b_1(\pi^*) \leftarrow 2b_1(\pi)$ (58%) $2a_2(\pi^*) \leftarrow 1a_2(\pi)$ (35%)
1^1A_1	$s \leftarrow n$	50 651		52 141	0.001	$12\ a_1 \leftarrow 11a_1(n)$ (99%)
2^1B_2	$\pi^* \leftarrow \pi$	58 233		57 231	0.143	$2a_2(\pi^*) \leftarrow 2b_1(\pi)$ (43%) $8b_2(\sigma) \leftarrow 11a_1(n)$ (40%)

[a] SAOP(ALDA)/TZ2P(AE) at the BP86/TZP(FC) geometry. [b] Transition energy in inverse centimeters. [c] Oscillator strength.

molecules present in the background gas; however, the level of interaction was found to decline as the ion trap cooled and the water was removed via cryopumping. In addition, fragment ions were frequently observed to associate with background H_2O and N_2 (or possibly CO) to occupy the vacant site left by the photodetacted ligand molecule. To determine fractional photofragment yields, all ion signals related to either the precursor or the fragments were summed, respectively, to generate overall precursor and fragment ion intensities. As will be shown, the influence an additional water molecule has on a spectrum is minimal and is easily accounted for.

Magnesium required the comparatively low Knudsen cell temperature of 490 °C to generate sufficient metal vapor to balance sublimation of the metal for efficient pick up against the need to avoid scattering the molecular beam. For calcium, the optimum cell temperature was 590 °C, and for fresh strontium a strong pick up signal could be achieved at a cell temperature of 520 °C. Older samples of the metal required a slightly higher temperature to remove an oxide layer that can appear on the surface. In terms of ion injection into the trap, complexes of both magnesium and calcium behaved as expected; however, for those of strontium, the strong ion signals detected in the mass spectrometer did not, for reasons as yet unknown, translate into high number densities in the trap. Performance could be improved by increasing the helium pressure in the trap, but whether it was the case that $[Sr(L)_4]^{2+}$ ions required more helium collisions to reduce their momentum or whether it was merely the normal boost in signal that can come from increased helium pressure was not clear.[30]

THEORY SECTION

The structure, binding energy, and electronic excitation energies of the alkaline earth $[M(pyridine)_4]^{2+}$ complexes, M = Mg, Ca, and Sr, were calculated using density functional theory, as implemented in the Amsterdam density functional (ADF) program.[31−33] Geometry optimization and frequency calculations were performed using the local density approximation (LDA) due to Vosko et al.[34] together with the gradient-corrected exchange of Becke[35] and the correlation correction of Perdew[36] (BP86), with a Slater-type orbital basis set of triple-ζ plus polarization (TZP) and with default convergence criteria. The Mg complex calculations were performed at the all-electron level, whereas the Ca and Sr complex calculations were performed with a small frozen core (the core orbital up to Ca2p, Sr3p, C1s, N1s and O1s were set as core orbitals). For $[Sr(pyridine)_4]^{2+}$, relativistic effects were taken into account using the zeroth order regular approximation (ZORA).[37] Excitation energies and oscillator strengths are calculated using

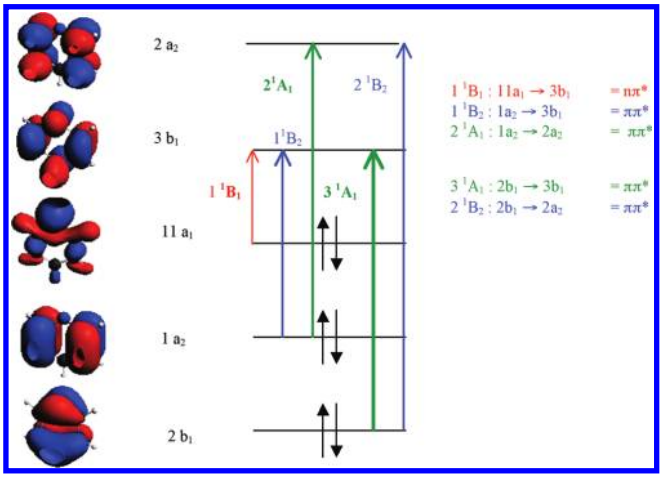

Figure 3. Schematic diagram showing the lowest-lying excited states of the pyridine molecule. These have been used to assign transitions in $[M(pyridine)_4]^{2+}$ where each pyridine in the metal complex exhibits the ligand orbitals involved in the state shown. The assignments are based on SAOP(ALDA)/TZ2P(AE) calculations. (See Table 1.)

time-dependent density functional theory (TDDFT), as implemented in ADF.[38−42] The asymptotically correct SAOP functional[43] with a TZ2P all-electron basis set was used in the SCF step and the adiabatic local density approximation (ALDA)[44] in the post SCF step for all complexes considered. Relativistic effects were incorporated via ZORA in the Sr complex calculations.

To aid analysis of the electronic excitations of $[M(pyridine)_4]^{2+}$ complexes and to validate the methodology, calculations have also been performed on the pyridine molecule using the same level of theory (SAOP(ALDA)/TZ2P(AE)). In Table 1, these results are compared with experimental excitation energies taken from gas-phase UV absorption spectra.[45] The calculations compare vertical excitations, as predicted by adiabatic TDDFT with the experimental band maxima, and no account of vibrational coupling has been considered. Calculated excitations are assigned according to the orbitals involved in each transition. The $\pi^* \leftarrow n$ transition ($^1B_1$) and the $\pi^* \leftarrow \pi$ transitions ($^1B_2$, and two $^1A_1$) are all in very good agreement with experiment, in terms of both excitation energy (errors <0.3 eV) and the relative magnitudes of the oscillator strengths.[46] The experimental splitting between the first $^1A_1$ (reported as $s \leftarrow n$ by Walker et al.[47]) and the second $^1A_1$ ($\pi^* \leftarrow \pi$) is just 0.1 eV. The calculation reverses the order of these two states, and so Table 1 is labeled in terms of the experimental assignment (i.e., the $\pi^* \leftarrow \pi$ $^1A_1$ transitions are labeled

Table 2. Calculated Incremental Binding Energies, *BE*(pyridine) (kJ mol^{-1} and cm^{-1}), at the BP86/TZP Level of Theory, Including Zero-Point Energy Correction: $[M(pyridine)_4]^{2+} \rightarrow [M(pyridine)_3]^{2+} + Pyridine$[a]

complex	symm	*BE*(pyridine)/kJ mol^{-1}	*BE*(pyridine)/cm^{-1}	*R*[M^{2+}−N]/pm	∠N−M^{2+}−N/°
$[Mg(pyridine)_4]^{2+}$	D_{2d}	178	14,870	210 (4)	110 (4)
					109 (2)
	$\sim S_4$	183		210 (4)	111 (4)
					106 (2)
$[Mg(pyridine)_3]^{2+}$	D_3			206 (3)	120 (3)
$[Ca(pyridine)_4]^{2+}$	D_{2d}	163	13,655	240 (4)	108 (4)
					113 (2)
	$\sim S_4$	167		240 (4)	111 (4)
					106 (2)
$[Ca(pyridine)_4(H_2O)]^{2+}$	$\sim C_s$			246 (2)	106 (2)
				244	93 (2)
				242	104
					145
$[Ca(pyridine)_3]^{2+}$	D_{3h}			237 (3)	120 (3)
$[Sr(pyridine)_4]^{2+}$	D_{2d}	147	12,280	258 (4)	109 (4)
					113 (2)
	$\sim S_4$	149		257 (4)	111 (4)
$[Sr(pyridine)_3]^{2+}$	D_3			254 (3)	120 (3)

[a] Sr data include relativistic effects via ZORA. Metal(N)−nitrogen(N) bond lengths (*R*/pm) and N−M−N bond angles (∠/°) are also given. Degeneracy is given in parentheses. The Ca−OH_2 bond length is 242 pm.

2^1A_1 and 3^1A_1). Figure 3 shows the nature of the orbitals involved in each excitation step. It was found that in the $[M(pyridine)_4]^{2+}$ complexes each molecule engages the same ligand orbitals in each excitations; for example, all pyridine molecules display the same "2 + 2" interaction (ligand orbital $1a_2$) simultaneously. Depending on the relative phases exhibited by each pyridine molecule in a complex, several $[M(pyridine)_4]^{2+}$ molecular orbitals involve the $1a_2$ ligand orbital. For the lower symmetry complexes (S_4 and $[Ca(pyridine)_4(H_2O)]^{2+}$, see below), the $1a_2$ ligand orbital (electron density) does not necessarily appear on all four pyridine molecules simultaneously. However, because of the distinct involvement of pyridine ligand molecular orbitals (as depicted in Figure 3), it has been possible to classify each metal-complex excitation in terms of the corresponding pyridine molecule excitation. Only excitations appropriate for a discussion of the metal complexes are depicted in Figure 3.

■ CALCULATED GEOMETRIC PROPERTIES OF $[M(PYRIDINE)_{3,4}]^{2+}$ COMPLEXES

Two near-degenerate low-energy structures of the four-coordinate complexes were found and confirmed as minima by frequency analysis for all of the metal complexes considered. The structure of the pyridine ligand is such that it is not possible for any of the closed-shell complexes to adopt a perfect tetrahedral geometry. Instead, calculations show the presence of a D_{2d} structure and a lower symmetry structure that differs from D_{2d} by reorientation of the pyridine ligands to give a structure that is approximately S_4 symmetry but has been optimized without symmetry constraints. The energy difference between these structures is <4 kJ mol^{-1} for all three $[M(pyridine)_4]^{2+}$ complexes, with the S_4 geometry being slightly more stable. Given this small difference, electronic transitions arising from both structures should be observed in the photoexcitation experiments. Calculations have also been performed on $[Ca(pyridine)_4(H_2O)]^{2+}$, which was found to be approximately C_s symmetry, and on $[M(pyridine)_3]^{2+}$ complexes, M = Mg, Ca, and Sr, to determine the binding energy of a fourth ligand in the four-coordinate structures. The D_{3h} geometry was confirmed as a minimum for the $[Ca(pyridine)_3]^{2+}$ complex, and all D_3 symmetry $[M(pyridine)_3]^{2+}$ complexes, M = Mg, Ca and Sr, were confirmed as minima by the absence of imaginary vibrational modes.

Geometric parameters for $[M(pyridine)_{3,4}]^{2+}$ (M = Mg, Ca, and Sr) and $[Ca(pyridine)_4(H_2O)]^{2+}$ complexes are given in Table 2, and pictorial examples of the two structural $[M(pyridine)_4]^{2+}$ isomers and the $[Ca(pyridine)_4(H_2O)]^{2+}$ complex are given in Figure 4. The metal−nitrogen bond length (M−N) increases on going from M = Mg to Ca to Sr, and this is attributed to differences in the ionic radii. Confirmation is found by subtracting the calculated bond length from either the Pauling M(II) radius (Mg = 65, Ca = 99, Sr = 113 pm) or the reported six-coordinate M(II) radius (Mg = 86, Ca = 114, Sr = 132 pm) (http://www.webelements.com/). A shorter bond length enhances the electrostatic interaction, and this together with differences in electronegativity of the metals concerned (Mg > Ca ≥ Sr) results in significant differences in binding energy. Incremental (ligand) binding energies, defined as the energy required to perform the step $[ML_N]^{2+} \rightarrow [ML_{N-1}]^{2+} + L$, are given in Table 2 and include zero-point energy corrections. The results show that the binding energies of the fourth pyridine ligand decrease with increasing atomic radius of the dication and that in all cases the binding (or dissociation) energy is very much less than the wavelength used to photoexcite a complex.

■ RESULTS AND DISCUSSION

Several trends are visible in the ion trap photofragmentation mass spectra shown in Figure 2, the foremost being the increased propensity of a trapped dication complex (and some of the photofragments) to pick up one or more water molecules as the ionic radii of the metal ions increase. This behavior reaches a

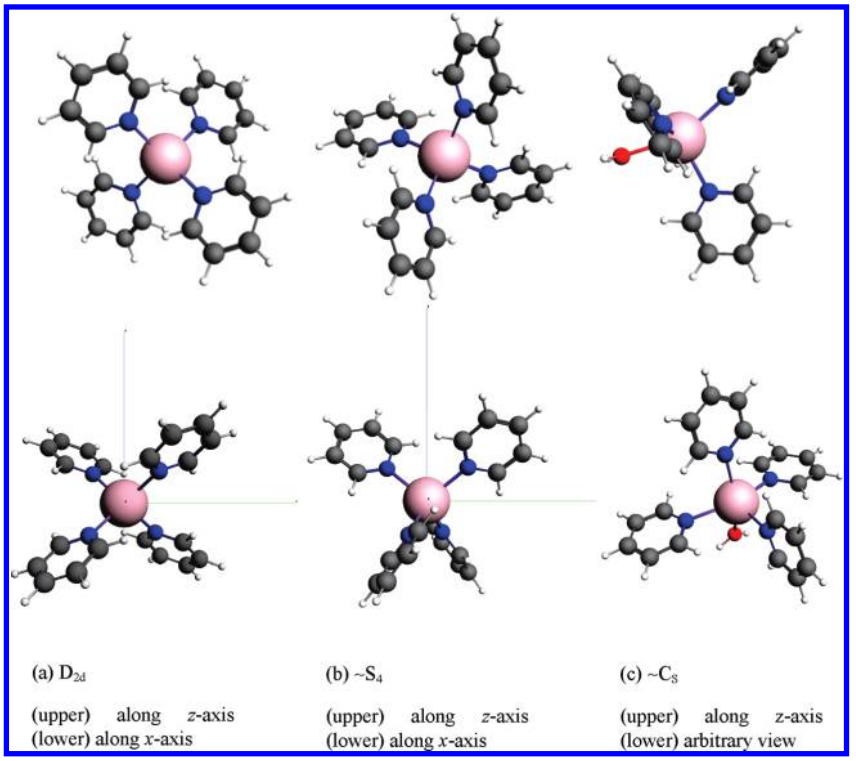

Figure 4. Optimized structures (BP86/TZP) (a) D_{2d} $[Ca(pyridine)_4]^{2+}$, (b) S_4 $[Ca(pyridine)_4]^{2+}$, which are representative of the same symmetry $[Mg(pyridine)_4]^{2+}$ and $[Sr(pyridine)_4]^{2+}$ complexes, and (c) $[Ca(pyridine)_4(H_2O)]^{2+}$.

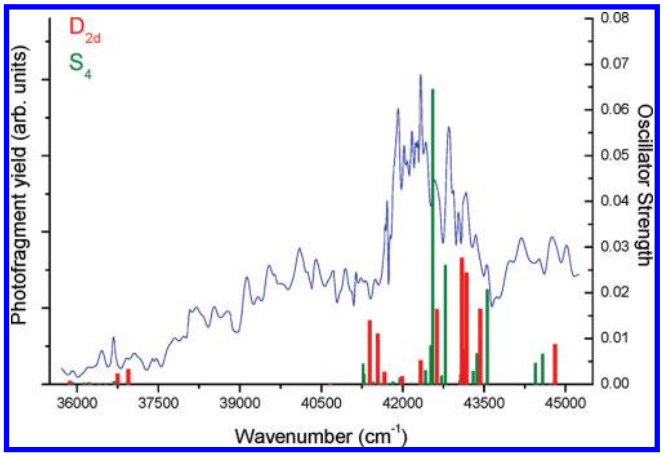

Figure 5. UV photofragment spectrum of $[Mg(pyridine)_4]^{2+}$ overlaid with calculated allowed transitions for D_{2d} and S_4 structures.

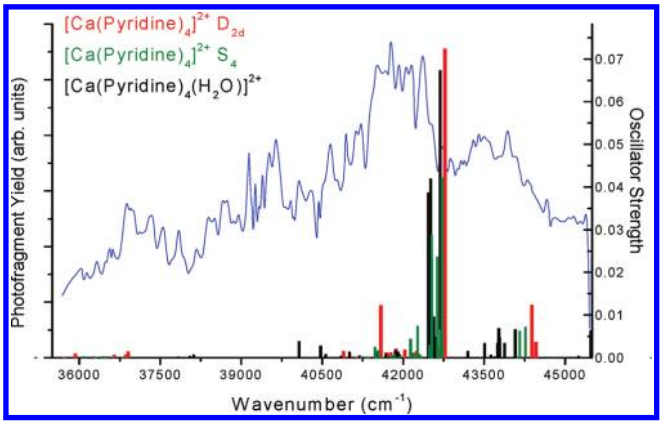

Figure 6. UV photofragment spectrum of $[Ca(pyridine)_4]^{2+}$ overlaid with calculated allowed transitions for both $[Ca(pyridine)_4]^{2+}$ D_{2d} and S_4 structures and for $[Ca(pyridine)_4(H_2O)]^{2+}$.

point where the ions $[Ca(pyridine)_4]^{2+}$ and $[Ca(pyridine)_4(H_2O)]^{2+}$ have equivalent intensities over the course of an experiment, and $[Sr(pyridine)_4(H_2O)]^{2+}$ is frequently the dominant species. The appearance of a strong protonated pyridine (pyridine-H^+) signal is predominantly a feature of mass spectra recorded from $[Mg(pyridine)_4]^{2+}$. In a previous study of $[Mn(pyridine)_4]^{2+}$, the formation of pyridine-H^+ was successfully monitored as a function of laser wavelength and taken to indicate the presence of photoinduced charge transfer.[17] However, $[Mg(pyridine)_4]^{2+}$ proved to be susceptible to interactions with background gas in the ion trap and underwent collision-induced dissociation, most probably with water, to produce pyridine-H^+.

Experimental photofragmentation spectra for $[Mg(pyridine)_4]^{2+}$, $[Ca(pyridine)_4]^{2+}$, and $[Sr(pyridine)_4]^{2+}$ are presented in Figures 5−7 respectively, and for the purposes of comparing the data, all three spectra are presented together in Figure 8. Also shown in Figure 8 is the location of a $\pi^* \leftarrow \pi$ transition taken from the experimental UV spectrum of neutral pyridine.[45,47] It can be seen that across the range of metals the spectra are very similar in structure and share several common features. However, they are all dominated by a single strong transition at ~42 000 cm^{-1}, which exhibits a notable blue shift of several hundred wavenumbers as the metal center changes from Sr^{2+} through Mg^{2+}. Given the position of the $\pi^* \leftarrow \pi$ transition in neutral pyridine and the systematic blue shift induced by the presence of a metal dication, it is quite probable

dx.doi.org/10.1021/jp112171j |J. Phys. Chem. A 2011, 115, 6948–6960

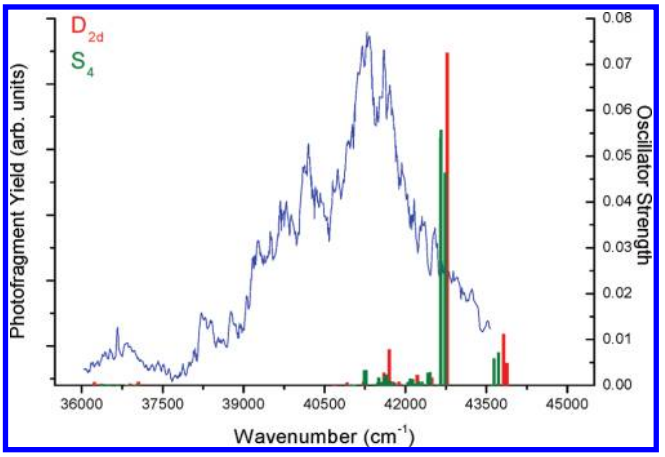

Figure 7. UV photofragment spectrum of $[Sr(pyridine)_4]^{2+}$ overlaid with calculated allowed transitions for D_{2d} and S_4 structures.

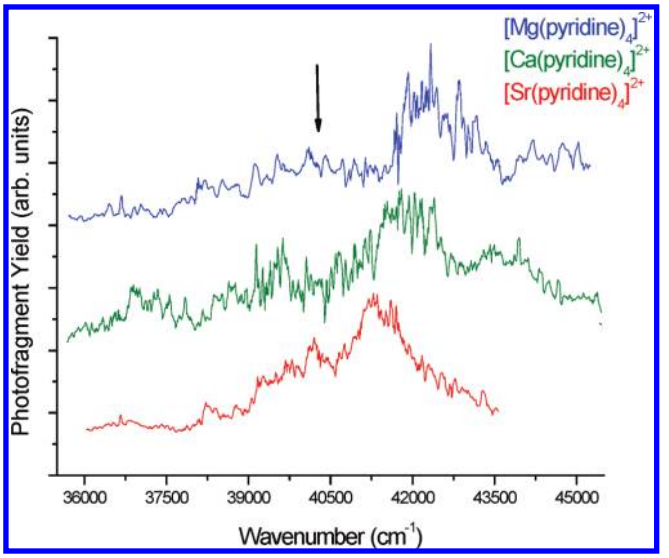

Figure 8. Combined experimental photofragment spectra for the Group II metal−pyridine dication complexes. An arrow denotes the position of the most intense $\pi^* \leftarrow \pi$ transition in neutral pyridine that appears in this region of the spectrum.

(see below) that the most prominent feature in the experimental spectra is a blue shift $\pi^* \leftarrow \pi$ transition based on one or more of the ligands. In some cases, the spectra clearly contain up to four resolved features, and these also shift according to the metal center. Variations in the weaker features between spectra may come as a consequence of differing structures, the increasing presence of additional water ligands in the heavier complexes, or both. However, accurate identification of some of these features is hampered by a poor signal-to-noise ratio.

Also present in Figures 5−7 are stick spectra that have been calculated using the methods outlined above. Calculated excitation energies and oscillator strengths for both the D_{2d} and S_4 geometries (the latter without symmetry constraint) of the $[M(pyridine)_4]^{2+}$ complexes are plotted, together with comparable data calculated for the $[Ca(pyridine)_4(H_2O)]^{2+}$ complex (Figure 6). In agreement with the experimental results, no excitations are predicted to occur below 35 000 cm^{-1} in any of the complexes. The first electronic transitions are predicted to occur at ∼36 000 cm^{-1} (Mg complex: (E = 35 870 cm^{-1}, f = 0.0006); Ca complex (E = 35 929, cm^{-1}, f = 0.0009), Sr complex (E = 36 235 cm^{-1}, f = 0.0006)). These oscillator strengths, f, are nearly two orders of magnitude smaller than the strongest (f = 0.07), and so it is assumed that these transitions are unlikely to be observed experimentally; however, they could give rise to vibrational coupling. For all of the complexes, differences between spectra calculated for the D_{2d} and S_4 geometries are sufficiently small that both map closely on to the experimental features, making it difficult to differentiate between the two; however, for $[Mg(pyridine)_4]^{2+}$, the D_{2d} results do provide a better fit to the overall spectrum. In particular, it can be seen that there are transitions calculated for a D_{2d} structure that match several of the weaker features seen in the experimental spectrum.

Table 3 summarizes the electronic transitions calculated to dominate the UV spectra of both structural isomers of the $[M(pyridine)_4]^{2+}$ complexes and of $[Ca(pyridine)_4(H_2O)]^{2+}$. The table shows only those transitions that are calculated to fall within the experimental wavelength range and have $f > 0.01$. Also given is a state assignment for the photoexcited complex and the corresponding molecular state occupied by each pyridine involved in the metal-complex transition. Tables S1−S3 in the Supporting Information contain the dominant electronic transitions in $[M(pyridine)_4]^{2+}$ complexes (M = Mg, Ca and Sr) (oscillator strength, $f \geq 0.003$ for the D_{2d} symmetry and $f > 0.01$ for the lower symmetry structures). Also given are the orbitals involved in a transition, the weight of the contribution each transition makes to that excitation (weight >5%), and an assignment of the nature of the excitation, with reference to the pyridine molecule state from which it is derived.

It is clear that for all of the metal complexes considered, the strongest transitions predicted by TDDFT fall within a narrow band, 41 000−43 000 cm^{-1}, and are in good agreement with the principal experimental peaks observed at ∼42 000 cm^{-1}. Excitations arising from D_{2d} complexes show a slight (but insignificant) blue shift of the most intense transition with decreasing atomic number (highlighted in bold in Table 3), as observed experimentally. The strongest transition in the D_{2d} $[Ca(pyridine)_4]^{2+}$ and $[Sr(pyridine)_4]^{2+}$ complexes is a ^1E state with an oscillator strength of 0.07 and excitation energies of 42 776 and 42 774 cm^{-1}, respectively. In both cases, the transition is derived from the 1^1B_2 state of the pyridine molecule and is thus a $\pi^* \leftarrow \pi$ transition. The strongest D_{2d} $[Mg(pyridine)_4]^{2+}$ transition is also a ^1E state but has a smaller oscillator strength of 0.03 and an excitation energy of 43 091 cm^{-1}. The transition is of mixed symmetry, with the largest contribution coming from the 1^1B_1 state of the pyridine molecule ($\pi^* \leftarrow$ n); however, there are also significant contributions from the 2^1A_1 and 1^1B_1 states that are $\pi^* \leftarrow \pi$ in nature. This mixing could imply double- or higher-excitation character in this state. Although adiabatic TDDFT contains only the single excitation manifold, it has been shown (by comparison with CASPT2 calculations)[48] that mainly singly excited states with a large contribution from doubly excited configurations do appear, and their excitation energy is no less accurate than the pure singly excited states. All other $[Mg(pyridine)_4]^{2+}$ excitations given in Table 3 derived from the D_{2d} complex, although involving several transitions, are of a single character/nature.

It is pertinent to note that spectra calculated for the $[Ca(pyridine)_4]^{2+}$ and $[Sr(pyridine)_4]^{2+}$ complexes with D_{2d} geometry are qualitatively similar in that they both involve one dominant transition accompanied by 1 or 2 weaker transitions. In contrast, the $[Mg(pyridine)_4]^{2+}$ spectrum is calculated to contain twice as many transitions (within the experimental wavelength

dx.doi.org/10.1021/jp112171j |J. Phys. Chem. A 2011, 115, 6948–6960

Table 3. Dominant Electronic Transitions ($f > 0.01$) Calculated for $[Mg(pyridine)_4]^{2+}$, $[Ca(pyridine)_4]^{2+}$, and $[Sr(pyridine)_4]^{2+}$ Complexes and for the $[Ca(pyridine)_4(H_2O)]^{2+}$ Complex[a]

metal	complex symmetry	state	E[b]	f[c]	assignment	pyridine[d]
Mg	D_{2d}	^{1}E	41 395	0.01	$\pi^* \leftarrow \pi$	2 $^1A_1$
		^{1}E	41 539	0.01	$\pi^* \leftarrow \pi$	3 $^1A_1$
		^{1}E	42 632	0.02	$\pi^* \leftarrow$ n	1 $^1B_1$
		^{1}E	**43 091**	**0.03**	**$\pi^* \leftarrow$ n/$\pi^* \leftarrow \pi$**	**1 $^1B_1$/2 $^1A_1$ /1 $^1B_2$**
		^{1}E	43 178	0.02	$\pi^* \leftarrow \pi$	2 $^1A_1$
		^{1}E	43 431	0.02	$\pi^* \leftarrow$ n	1 $^1B_1$
	$\sim S_4$[e]	$\sim ^1$E[e]	**42 555**	**0.06**	**$\pi^* \leftarrow \pi$**	**1 $^1B_2$/2 $^1A_1$**
			42 786	0.03	$\pi^* \leftarrow \pi$	1 $^1B_2$/2 $^1A_1$
			43 557	0.02	$\pi^* \leftarrow$ n	1 $^1B_1$
Ca	D_{2d}	^{1}E	41 585	0.01	$\pi^* \leftarrow \pi$	2 $^1A_1$
		^{1}E	**42 776**	**0.07**	**$\pi^* \leftarrow \pi$**	**1 $^1B_2$**
		$^1B_2$	44 383	0.01	$\pi^* \leftarrow$ n	1 $^1B_1$
	$\sim S_4$[e]		42 527	0.03	$\pi^* \leftarrow \pi$	2 $^1A_1$/1 $^1B_2$
			42 531	0.02	$\pi^* \leftarrow \pi$	2 $^1A_1$/1 $^1B_2$
		$\sim ^1$E[e]	42 632	0.02	$\pi^* \leftarrow \pi$	2 $^1A_1$/1 $^1B_2$
			42 720	**0.04**	**$\pi^* \leftarrow \pi$**	**1 $^1B_2$**
$Ca \cdot H_2O$	$\sim C_s$[e]		42 464	0.04	$\pi^* \leftarrow \pi$	1 $^1B_2$ (2 $^1B_2$)
			42 510	0.04	$\pi^* \leftarrow \pi$	1 $^1B_2$ (2 $^1B_2$)
			42 687	**0.07**	**$\pi^* \leftarrow \pi$**	**1 $^1B_2$ (2 $^1B_2$)**
Sr	D_{2d}	**^{1}E**	**42 774**	**0.07**	**$\pi^* \leftarrow \pi$**	**1 $^1B_2$**
		$^1B_2$	43 817	0.01	$\pi^* \leftarrow$ n	1 $^1B_1$
	$\sim S_4$[e]		42 649	0.05	$\pi^* \leftarrow \pi$	1 $^1B_2$
			42 659	**0.06**	**$\pi^* \leftarrow \pi$**	**1 $^1B_2$**
			42 737	0.05	$\pi^* \leftarrow \pi$	1 $^1B_2$

[a] Strongest transition is shown in bold. No excited electronic state label is given for the S_4 or C_s geometries because these were optimized without symmetry and so all are of ^{1}A symmetry. [b] Transition energy in inverse centimeters. [c] Oscillator strength. [d] These assignments are derived for the isolated pyridine molecule and refer to Table 1 and Figure 3. Where a second state is shown in parentheses, it implies a minor contribution, for example, 1 $^1B_2$ (2 $^1B_2$), whereas a forward slash implies a comparable contribution, for example, 1 $^1B_2$/2 $^1A_1$, with the first state contributing the greater weight. [e] $\sim$ implies approximate symmetry (i.e., calculation performed without symmetry constraint).

range and with $f > 0.01$ but also when all $f \geq 0.003$ transitions are considered), which would imply that signal intensity is spread over a number of separate excitations. This change in behavior could be due to the additional mixing of pyridine molecule states seen in the dominant excitation for $[Mg(pyridine)_4]^{2+}$. From an experimental viewpoint, the photofragment signal intensity from $[Mg(pyridine)_4]^{2+}$ was noticeably weaker, which would support the presence of many transitions with each having a low oscillator strength. The greater density of transitions evident in the calculated spectrum also makes experimental assignment more difficult, especially when considering the additional effects of water and changes in geometry.

For dominant excitations within the $\sim S_4$ complexes, the strongest transitions seen for the Ca and Sr complexes are derived from the 1^1B_2 pyridine molecule state; however, for the Mg complex there is again a mixed symmetry transition, but this does include a large contribution from the 1^1B_2 state and is of a single nature, that is, $\pi^* \leftarrow \pi$. Possibly because of the reduced degree of mixing, the oscillator strength for this latter transition is greater than any of those calculated for the D_{2d} complex. Furthermore, it is interesting to note that the oscillator strengths are also larger in the $\sim S_4$ symmetry Sr complex than the Ca complex and that the former does not mix pyridine states whereas the latter does.

Particularly surprising from the results in Table 3 is the fact that the oscillator strengths, assignments, and wavenumber values for transitions in the $[Ca(pyridine)_4(H_2O)]^{2+}$ complex do not show marked differences from those for the $[Ca(pyridine)_4]^{2+}$ complexes. The H_2O appears to play no active part in any of the electronic transitions, and structural rearrangement of the pyridine ligands to accommodate the water ligand and the changing calcium coordination environment also has no notable influence on the calculated spectra. The absence of an electronic contribution from H_2O is probably to be expected on the grounds that any electronic transitions within the molecule occur at far higher energies than are being considered here. The molecule also has a much lower polarizability than pyridine; therefore, compared with the latter, there will be far less movement of electron density away from water toward the metal dication. For all three calcium complexes, the most intense band is derived from the 1^1B_2 state of the pyridine molecule and shifts by <100 cm^{-1} upon going from D_{2d} to $\sim S_4$ symmetry and through to the $[Ca(pyridine)_4(H_2O)]^{2+}$ complex. Furthermore, transitions in the D_{2d} complex involve electron density on all four pyridine molecules, whereas the comparable transition in $[Ca(pyridine)_4(H_2O)]^{2+}$ involves electron density on just two pyridine ligands. This behavior demonstrates that the ligand environment is having little effect on the ligand-based $\pi^* \leftarrow \pi$ transitions that are responsible for spectra in the Ca^{2+} complex. The calculated transition energy to the 1^1B_2 state in the pyridine molecule is 42 883 cm^{-1}, and so the effect of the metal and presence of 4 (or 2) ligands exhibiting

dx.doi.org/10.1021/jp112171j |J. Phys. Chem. A 2011, 115, 6948–6960

Table 4. Orbital Energies, ε (in electronvolts), of the D_{2d} Geometry $[M(pyridine)_4]^{2+}$, M = Mg, Ca, Sr (Using the Asymptotically Correct SAOP Functional Which Correctly Stabilizes the Orbital Energies Relative to Those Calculated Using the BP86 Functional), *l* = lumo and *h* = homo[a]

	$[Mg(pyridine)_4]^{2+}$			$[Ca(pyridine)_4]^{2+}$			$[Sr(pyridine)_4]^{2+}$		
	orbital	ε	derived[b]	orbital	ε	derived[b]	orbital	ε	derived[b]
l+5	9 a2	−11.64	2 a2	9 a2	−11.50	2 a2	9 a2	−11.38	2 a2
l+4	9 b1	−11.84	2 a2	9 b1	−11.63	2 a2	10 b1	−11.48	2 a2
l+3	24 b1	−11.86	2 a2	25 e1	−11.63	2 a2	27 e1	−11.48	2 a2
l+2	23 e1	−12.48	3 b1	24 e1	−12.25	3 b1	26 e1	−12.08	3 b1
l+1	15 e2	−12.58	3 b1	16 b2	−12.28	3 b1	18 b2	−12.09	3 b1
lumo	**16 a1**	**−12.63**	**3 b1**	**17 a1**	**−12.40**	**3 b1**	**19 a1**	**−12.21**	**3 b1**
homo	**8 a2**	**−16.99**	**1 a2**	**8 a2**	**−16.79**	**1 a2**	**8 a2**	**−16.65**	**1 a2**
h−1	22 e1	−17.06	1 a2	23 e1	−16.82	1 a2	25 e1	−16.67	1 a2
h−2	8 b1	−17.06	1 a2	8 b1	−16.83	1 a2	9 b1	−16.68	1 a2
h−3	21 e1	−17.65	2 b1	22 e1	−17.43	2 b1	24 e1	−17.22	11 a1
h−4	15 a1	−17.73	2 b1	15 e2	−17.45	11 a1	17 b2	−17.25	11 a1
h−5	14 b2	−17.74	2 b1	21 e1	−17.47	2 b1	23 e1	−17.29	2 b1
h−6	20 e1	−17.92	11 a1	16 a1	−17.48	11 a1	18 a1	−17.32	2 b1
h−7	13 e2	−17.95	11 a1	14 b2	−17.56	11 a1	16 b2	−17.35	2 b1

[a] Pyridine molecule orbital energies at the same level of theory are as follows (lumo+1: $2a_2 = -5.58$ eV; lumo: $3b_1 = -5.99$ eV; homo: $11a_1 = -10.27$ eV; homo-1: $1a_2 = -10.74$ eV; homo-2: $2b_1 = -11.38$ eV). [b] Derived pyridine orbital; that is, each pyridine ligand in the complex exhibits this symmetry found in the isolated pyridine molecule. (See Figure 3.)

the excitation simultaneously is to (negligibly) red shift the 1^1B_2 excitation by <200 cm^{-1}.

There are three pyridine-derived transitions involved in the electronic excitations displayed by the $[M(pyridine)_4]^{2+}$ complexes. The most prevalent is $\pi^* \leftarrow \pi$ leading to the 1^1B_2 state, and as mentioned above, this excitation shifts little when promoted in the presence of an alkali earth dication. A second $\pi^* \leftarrow \pi$ transition calculated to appear in the spectra of dication complexes goes to the 2^1A_1 state. The Sr complexes do not exhibit this excitation, but for the Mg and Ca complexes, the first transitions involving the 2^1A_1 state both occur at ~41 500 cm^{-1}, and there is a second pure transition in the Mg complex that also involves the 2^1A_1 state and is calculated to occur at 43 178 cm^{-1}. In the pyridine molecule, the calculated energy for this transition is 50 134 cm^{-1} (within 0.13 eV < 1500 cm^{-1} of experiment), and so in both cases, the presence of the metal and other pyridine molecules serves to red shift this excitation by ~7000 cm^{-1}. A third pyridine molecule excitation exhibited by the alkali earth metal complexes is $\pi^* \leftarrow$ n and goes to the 1^1B_1 state. As a pure excitation, this transition is seen at 42 632, 43 431, and 43 557 cm^{-1} in Mg complexes, at 44 383 cm^{-1} in a D_{2d} Ca complex, and at 43817 cm^{-1} in a D_{2d} Sr complex. As such, the transition experiences a considerable blue shift of at least 6000 cm^{-1} relative to its energy in the pyridine molecule (36 852 cm^{-1} calculated, which is within 0.02 eV of experiment).

Orbital energy differences can be considered as an (crude) approximation for excitations that are dominated by a single determinant, and this can be used to provide some insight into the calculated spectral shifts. Table 4 lists the frontier orbital energies of the D_{2d} complexes, along with the pyridine orbital involved in each molecular orbital to aid interpretation of the spectral assignment. The first singlet excitation in the free pyridine molecule is the $^1B_1$, which involves a transition from the homo to the lumo ($3b_1 \leftarrow 11a_1$) and occurs at ~37 000 cm^{-1}. The magnitude of the homo-lumo gap is very similar (within 0.1 eV) in all of the complexes and is very similar to that of the free pyridine molecule. However, because of the presence of the metal and the additional pyridine molecules there is a reordering of the ligand-based orbitals such that in the complexes the homo is derived from the 1 a_2 pyridine orbital. The 11 a_1 orbital (the nitrogen "lone pair") is stabilized by the presence of the metal and the additional ligands. It is stabilized most in the Mg complex (where it is six orbitals below the homo and labeled h−6 in Table 4) and has a negligible (<2%) interaction with the Mg p orbitals. In the Ca complex, the first occupied molecular orbital involving the pyridine molecule orbital 11 a_1 is the homo−4, and in Sr, it is the homo−3, both of which have negligible (<4%) metal d orbital contribution. For all complexes, the lumo is derived from the 3 b_1 orbital, in keeping with the observed ordering in the free pyridine molecule. Thus, a qualitative explanation for the blue shift of the $^1B_1$ state is the fact that the 11 a_1 orbital is stabilized in each metal complex, which results in a larger energy gap than that in the free pyridine molecule. This blue shift moves the absorption energy into the region of the band maximum observed in the experiment.

In the free pyridine molecule, the $^1B_2$ state involves a transition from the homo-1 to the lumo, $3b_1 \leftarrow 1a_2$ (with a weak contribution from the $2a_2 \leftarrow 2b_1$), and in the metal complexes, the calculated transitions arising from the $^1B_2$ state are only slightly shifted (TDDFT shifts <300 cm^{-1}). In the metal complex, the homo, homo-1, and homo-2 all exhibit the 1 a_2 orbital on each pyridine (the molecular orbital energy difference arising from the relative phases of pyridine ligand orbitals) and, given that the energy of the homolumo gap in the free molecule and in the complexes is reasonably similar, this state exhibits minimal shift. Furthermore, the 1 a_2 orbital does not involve electron density on the nitrogen atom and so will be little affected directly by the presence of the metal. The dominant transitions in each of the complexes involve this state, and so this latter point provides a possible explanation for the similarity of the experimental and calculated band maxima.

Finally, the $2\ ^1A_1$ in the free pyridine molecule is red-shifted in the metal complexes. However, this $\pi^* \leftarrow \pi$ state in the pyridine molecule involves a strong configuration mixing of two diabatic

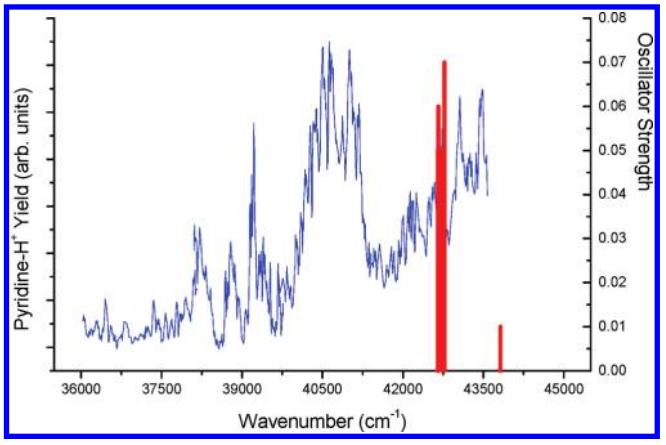

Figure 9. Contribution from the pyridine-H^+ signal to the spectrum for $[Sr(pyridine)_4]^{2+}$. Also shown are the calculated transitions selected from Table 3.

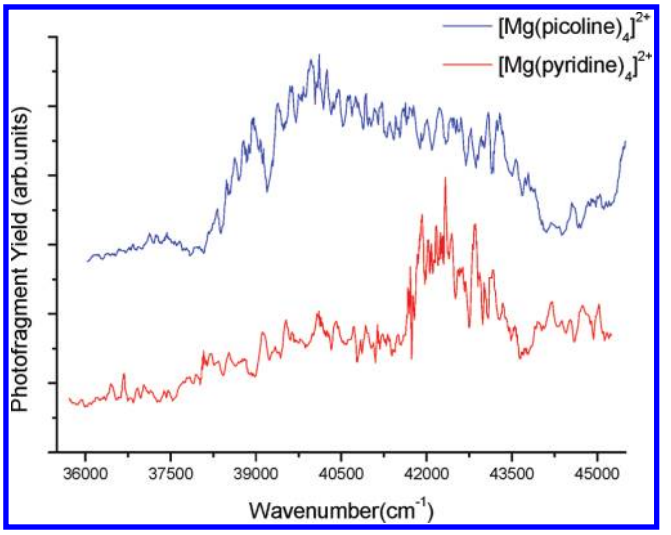

Figure 10. Comparison between the UV photofragment spectra of $[Mg(pyridine)_4]^{2+}$ (bottom) and $[Mg(4\text{-picoline})_4]^{2+}$ (top).

states ($2a_2 \leftarrow 1a_2$ and $3b_1 \leftarrow 2b_1$), and in both the free pyridine molecule and in the metal complexes, the orbital energy differences are not representative of the energy of this state. In both cases, the free pyridine and the metal complexes, the orbital energy differences are comparable ($\sim$42 000 cm^{-1}) but substantially less than the calculated free pyridine molecule 2^1A_1 excitation of 50 134 cm^{-1} which compares extremely well with the experimental value of 51 458 cm^{-1}. Thus, the calculated red shift could possibly be due to a reduced mixing of determinants (diabatic states) in the metal complexes.

Thus, it is clear from the TDDFT calculations that the dominant excitation in the observed spectra is due to a $\pi^* \leftarrow \pi$ transition derived primarily from the $^1B_2$ state of the pyridine molecule. The weaker features observed are attributed to the $\pi^* \leftarrow n\ ^1B_2$ state and the $\pi^* \leftarrow \pi\ ^1A_1$ state of the pyridine molecule, and a rationalization of the spectral shifts required to bring the absorption energy of these states into the region of the band maxima of the observed spectra of the dication complexes is given. However, this analysis does not necessarily account for the shift seen in Figure 8; although the most prominent $\pi^* \leftarrow \pi$ transition (1^1B_2) of the D_{2d} complexes is blue-shifted, as observed experimentally, and can be understood qualitatively in terms of the increasingly strongly perturbing metal dication, the calculated shift is insignificant (and is not reflected in the S_4 complexes). Furthermore, the extent of both the calculated shifts and the experimental shift is within the error bound of the calculations.

Although the calculated binding energy of the fourth ligand in each complex does decline as the central dication increases in size (Table 2), the comparatively low overall value for this energy would suggest that any variation is not responsible for the observed red shift. We would propose that photon absorption and fragmentation are quite separate events and that each complex, once it has absorbed a photon, probably has sufficient time to undergo radiative and/or nonradiative decay back to the ground state before fragmenting. Part of the reasoning behind this proposal is the fact that excitations are localized on the ligands and as such may not have a significant influence on the overall binding energy or stability of a complex. This proposed pattern of behavior is different from that identified by Choi et al.[20] as being responsible for the observed red shift in their alkaline earth dication spectra.

The above analysis closely matches the results from a previous study of the $[Zn(pyridine)_4]^{2+}$ UV spectrum.[12] There it was concluded that two principal pyridine molecular transitions could be identified as making a significant contribution to the observed spectrum. These were a $^1A_1\ \pi^* \leftarrow \pi$ transition that was red-shifted into the wavelength region studied and a $^1B_1\ \pi^* \leftarrow n$ transition that had been blue-shifted.[12] A second $\pi^* \leftarrow \pi$ transition ($^1B_2$) was also considered to be the source of two smaller features seen in the spectrum. However, as noted above, the $[Zn(pyridine)_4]^{2+}$ spectrum was also found to contain a series of comparatively intense features that were assigned as MLLCT (metal/ligand-to-ligand charge transfer) transitions. Clearly, the effect a dication has on $\pi^* \leftarrow n$ transitions can be attributed to coordination of pyridine to the metal ion via the lone pair electrons on the nitrogen atom. As the combined spectrum in Figure 8 shows, the extent of the shifts varies within the series of dications and on going from Mg^{2+} through to Sr^{2+}, the spectra exhibit a distinct red shift, which from the above analysis would suggest that $\pi^* \leftarrow \pi$ transitions contribute to this processes.

In a previous study of the $[Mn(pyridine)_4]^{2+}$ spectrum,[17] the appearance of protonated pyridine, (pyridine-H^+) as a photofragment was equated to ligand−metal charge transfer taking place as the result of excitation. For reasons discussed above, the corresponding process in $[Mg(pyridine)_4]^{2+}$ could not be monitored, and for $[Ca(pyridine)_4]^{2+}$, there was evidence of a similar but lesser effect. As noted above, collisions with water within the ion trap could, in part, be responsible for the appearance of pyridine-H^+, and a previous study of $[Mg(pyridine)_n]^{2+}$ complexes conducted under UHV conditions did not show any evidence of the ion.[49] The $[Ca(pyridine)_4]^{2+}$ complex did, however, exhibit a gradual increase in pyridine-H^+ signal as a function of photon energy. In contrast with this lack of structure, Figure 9 shows that by monitoring the appearance of pyridine-H^+ in the spectrum of $[Sr(pyridine)_4]^{2+}$, the presence of a large feature at 40 800 cm^{-1} can be seen, and this is accompanied by an increased signal at higher photon energies that is similar to that seen for $[Ca(pyridine)_4]^{2+}$. As with $[Mn(pyridine)_4]^{2+}$, the appearance of pyridine-H^+ does not correlate exactly with any of the transitions that dominate the photofragment spectra. However, there is some overlap between the appearance of pyridine-H^+ and $\pi^* \leftarrow \pi$ transitions predicted to appear at high photon energies for both the calcium and strontium dication complexes. Because doubly charged calcium and strontium do not possess unpaired d-electrons, the extent of ligand−metal

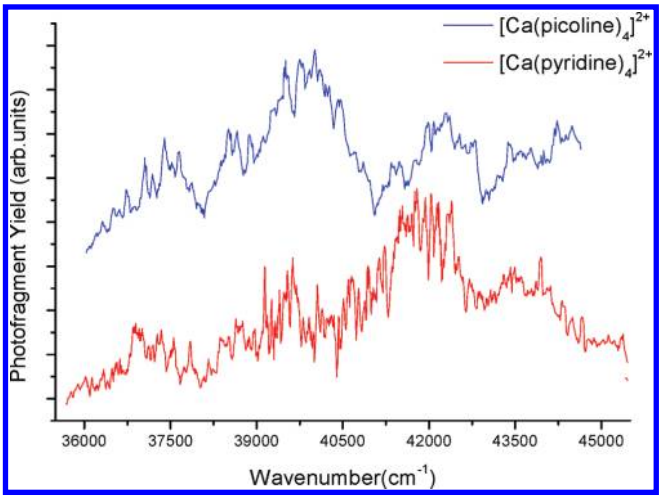

Figure 11. Comparison between the UV photofragment spectra of $[Ca(pyridine)_4]^{2+}$ (bottom) and $[Ca(4\text{-picoline})_4]^{2+}$ (top).

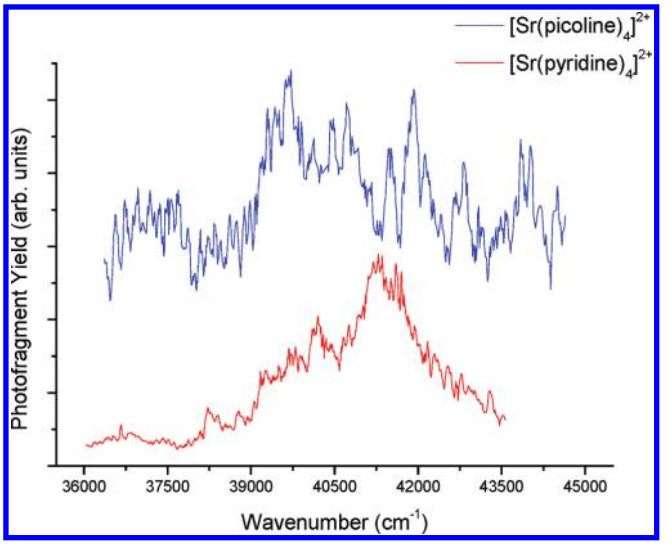

Figure 12. Comparison between the UV photofragment spectra of $[Sr(pyridine)_4]^{2+}$ (bottom) and $[Sr(4\text{-picoline})_4]^{2+}$ (top).

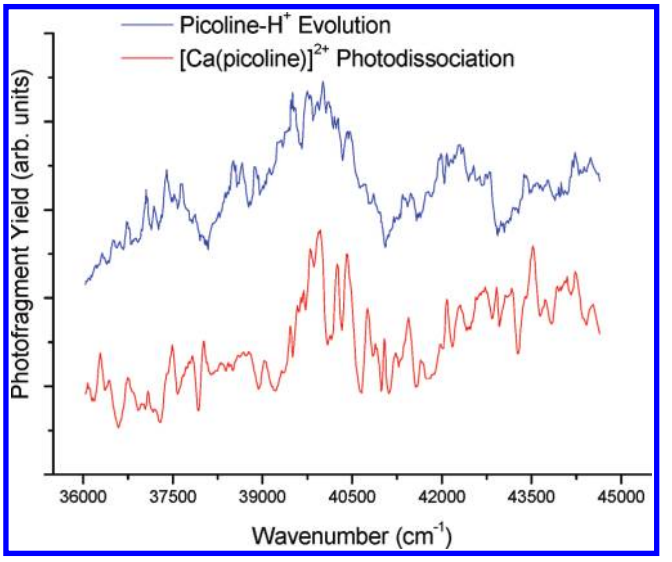

Figure 13. Comparison between the UV photofragment spectrum for $[Ca(4\text{-picoline})_4]^{2+}$ (top) and the signal recorded for 4-picoline-H^+.

charge transfer within the excitation itself is going to be, as the calculations show, minimal. One possibility is that there is a curve crossing within the excited state of the complex that correlates with charge transfer products appearing at the reaction asymptote. Contributions from the electronic excitation and fragmentation of the $[Ca(pyridine)_4\,(H_2O)]^{2+}$ complex to give pyridine-H^+ cannot be ruled out; however, the corresponding counterion, Ca^+OH-$(pyridine)_3$, was not observed.

A series of identical experiments to those described above was also undertaken on metal-4-picoline complexes in the form of $[Mg(4\text{-picoline})_4]^{2+}$, $[Ca(4\text{-picoline})_4]^{2+}$, and $[Sr(4\text{-picoline})_4]^{2+}$. Figures 10−12 show these results presented in the form of a comparison between the 4-picoline results and the corresponding pyridine data for each of the metal dications. For reasons unknown, the spectrum recorded for $[Mg(4\text{-picoline})_4]^{2+}$ is not particularly well-resolved and in fact the profile shown is quite similar to that of the UV spectrum for 4-picoline. The relationship between the three picoline spectra is very similar to that identified for the pyridine complexes in that there is a small red shift in the principal features as the series moves from magnesium through strontium. At first sight, the metal−picoline spectra would appear to have gained an intense feature at ∼40 000 cm^{-1}, which is reflective of the additional structure present in the UV spectrum of pure 4-picoline vapor when compared with that of pyridine.[50] A dominant feature of the metal−pyridine spectra at 42 000 cm^{-1} is retained in all of the metal−picoline spectra, albeit masked in the case of $[Mg(4\text{-picoline})_4]^{2+}$ because of a lack of resolution. The only reference point available for 4-picoline is a vapor phase spectrum,[50] and compared with that the dication spectra show a slight blue shift, which, based on the pyridine results, is to be expected. Because a methyl group in the four-position on pyridine should be electron-donating to the ring, comparable features seen in the pyridine spectrum might be expected to be red-shift in 4-picoline, which is certainly true of the spectra record for the vapor. Therefore, there are two possibilities for the structure seen, for example, in Figure 11 for Ca^{2+}. Either the entire spectrum for $[Ca(4\text{-picoline})_4]^{2+}$ has shifted to the red and additional features appear to the blue because they now fall within the UV range of the laser, or, alternatively, electron donation enhances the oscillator strengths of certain $\pi^* \leftarrow \pi$ and $\pi^* \leftarrow$ n transitions beyond what is seen for pyridine in the same environment. Possibly the most significant feature of these measurements of the spectra of 4-picoline complexes is that they exhibit structure and that it is different from that observed for the equivalent pyridine complexes; such behavior was not seen in previous measurements taken from complexes that remained hot.[10]

The protonated 4-picoline ion, 4-picoline-H^+, was observed as a photofragment in the case of both $[Mg(4\text{-picoline})_4]^{2+}$ and $[Ca(4\text{-picoline})_4]^{2+}$, where in each a structured feature was observed against the general trend of an increasing 4-picoline-H^+ signal. For $[Mg(4\text{-picoline})_4]^{2+}$, a peak is somewhat unexpected given the lack of resolution seen in Figure 10, but the transition could easily coincide with processes taking place under the profile recorded for that ion. Figure 13 compares the 4-picoline-H^+ signal with the profile recorded from a summation of all photofragments seen for $[Ca(4\text{-picoline})_4]^{2+}$, and in this case, there is overlap with at least one dominant feature. As with $[Sr(pyridine)_4]^{2+}$, this feature would suggest the presence of a

dx.doi.org/10.1021/jp112171j |J. Phys. Chem. A 2011, 115, 6948–6960

curve crossing from the excited state of the complex. Evolution of 4-picoline-H^+ signal from $[Sr(4\text{-picoline})_4]^{2+}$ was also monitored, but a very poor signal-to-noise ratio makes it difficult to draw any conclusions from the data.

CONCLUSIONS

A combination of the pick-up technique and ion trapping has been used to record UV photofragmentation spectra for a series of complexes consisting of alkaline earth metal dications in association with either pyridine or 4-methyl pyridine. As a consequence of cooling the ions, the spectra exhibit resolved features as a function of the wavelength of the UV radiation. A complementary series of TDDFT calculations is able to capture the essential features of the experimental photodissociation spectra. The wavelengths at which the complexes start to exhibit electronic transitions in the UV and wavelengths at which absorption maxima occur are both in good agreement with experiment, and it is possible to assign spectra based on ligand−ligand transitions. The more subtle features of the spectra, such as the spectral shift due to the change in dication, are less conclusive, and the magnitudes of these shifts lie within the error bars of the theoretical method.

ASSOCIATED CONTENT

Supporting Information. Comparison of the dominant electronic transitions ($f \geq 0.003$) in the D_{2d} $[Mg(pyridine)_4]^{2+}$, $[Ca(pyridine)_4]^{2+}$, and $[Sr(pyridine)_4]^{2+}$, comparison of the dominant electronic transitions ($f > 0.01$) in the ~S_4 $[Mg(pyridine)_4]^{2+}$, $[Ca(pyridine)_4]^{2+}$, and $[Sr(pyridine)_4]^{2+}$, and the dominant electronic transitions ($f > 0.01$) in $[Ca(pyridine)_4(H_2O)]^{2+}$. This material is available free of charge via the Internet at http://pubs.acs.org.

AUTHOR INFORMATION

Corresponding Author

*E-mail: anthony.stace@nottingham.ac.uk (experimental); h.cox@sussex.ac.uk (theory).

Present Addresses

[§]The Sericultural Research Institute, Chinese Academy of Agricultural Science, Zhenjiang Jiangsu 212018, China.

ACKNOWLEDGMENT

We would like to thank EPSRC and the University of Nottingham for financial support and the EPSRC National Service for Computational Chemistry Software for computer time: http://www.nsccs.ac.uk.

REFERENCES

(1) Lever, A. B. P. *Inorganic Electronic Spectroscopy*; Elsevier: Amsterdam, The Netherlands, 1984.
(2) Duncan, M. A. *Annu. Rev. Phys. Chem.* **1997**, *48*, 69.
(3) Fridgen, T. D. *Mass Spectrom. Rev.* **2009**, *28*, 586.
(4) Baer, T.; Dunbar, R. C. *J. Am. Soc. Mass Spectrom.* **2010**, *21*, 681.
(5) Spence, T. G.; Trotter, B. T.; Burns, T. D.; Posey, L. A. *J. Phys. Chem. A* **1998**, *102*, 6101.
(6) Thompson, C. J.; Husband, J.; Aguirre, F.; Metz, R. B. *J. Phys. Chem. A* **2000**, *104*, 8155.
(7) Puskar, L.; Stace, A. J. *J. Chem. Phys.* **2001**, *114*, 6499.
(8) Stace, A. J. *J. Phys. Chem. A* **2002**, *106*, 7993.
(9) Puskar, L.; Cox, H.; Goren, A.; Aitken, G. D. C.; Stace, A. J. *Faraday Discuss.* **2003**, *124*, 259.
(10) Guan, J.; Puskar, L.; Esplugas, R. O.; Cox, H.; Stace, A. J. *J. Chem. Phys.* **2007**, *127*, 064311.
(11) Bush, M. F.; Saykally, R. J.; Williams, E. R. *ChemPhysChem* **2007**, *8*, 2245.
(12) Wu, G.; Norris, C.; Stewart, H.; Cox, H.; Stace, A. J. *Chem. Commun.* **2008**, 4153.
(13) O'Brien, J. T.; Prell, J. S.; Steill, J. D.; Oomens, J.; William, E. R. *J. Phys. Chem. A* **2008**, *112*, 10823.
(14) Bush, M. F.; Oomens, J.; Saykally, R. J.; Williams, E. R. *J. Am. Chem. Soc.* **2008**, *130*, 6463.
(15) Dunbar, R. C.; Steill, J. D.; Polfer, N. C.; Oomens, J. *J. Phys. Chem. A* **2009**, *113*, 845.
(16) Mino, W. K.; Szczepanski, J.; Pearson, W. L.; Powell, D. H.; Dunbar, R. C.; Eyler, J. R.; Polfer, N. C. *Int. J. Mass Spectrom.* **2010**, *297*, 131.
(17) Wu, G.; Stewart, H.; Lemon, F. D.; Cox, H.; Stace, A. J. *Mol. Phys.* **2010**, *108*, 1199.
(18) Bush, M. F.; O'Brien, J. T.; Prell, J. S.; Wu, C. C.; Saykally, R. J.; William, E. R. *J. Am. Chem. Soc.* **2009**, *131*, 13270.
(19) Dunbar, R. C.; Hopkinson, A. C.; Oomens, J.; Siu, C. K.; Siu, K. W.; Steill, J. D.; Verkerk, U. H.; Zhao, J. *J. Phys. Chem. B* **2009**, *113*, 10403.
(20) Choi, C. M.; Lee, J. H.; Choi, Y. H.; Kim, H. J.; Kim, N. J.; Heo, J. *J. Phys. Chem. A* **2010**, *114*, 11167.
(21) Cox, H.; Stace, A. J. *Int. Rev. Phys. Chem.* **2010**, *29*, 555.
(22) Lippard, S. J. *The Principles of Bioinorganic Chemistry*; University Science Books: Mill Valley, CA, 1994.
(23) Fraústo da Silva; J. J. R.; Williams, R. J. P. *The Biological Chemistry of the Elements*; OUP: Oxford, U.K., 2001.
(24) Mizukami, S.; Okada, S.; Kimura, S.; Kikuchi, K. *Inorg. Chem.* **2009**, *48*, 7630.
(25) Groenewold, G.; Van Stipdonk, M. J.; Gresham, G. L.; Chien, W.; Bulleigh, K.; Howard, A. *J. Mass Spectrom.* **2004**, *39*, 752.
(26) Sudhir, P. R.; Wu, H. F.; Zhou, Z. C. *Rapid Commun. Mass Spectrom.* **2005**, *19*, 1517.
(27) James, P. F.; Perugini, M. A.; O'Hair, R. A. J. *Eur. J. Mass Spectrom.* **2007**, *13*, 433.
(28) Holmes, J. H.; Kleiber, P. D.; Olsgaard, D. A.; Yang, K. H. *J. Chem. Phys.* **2000**, *112*, 6583.
(29) Scott, A. C.; Buchanan, J. W.; Flynn, N. D.; Duncan, M. A. *Int. J. Mass Spectrom.* **2008**, *269*, 55.
(30) Wu, G.; Chapman, D.; Stace, A. J. *Int. J. Mass Spectrom.* **2007**, *262*, 211.
(31) *ADF2009.01*; SCM, Theoretical Chemistry, Vrije Universiteit: Amsterdam, The Netherlands. http://www.scm.com.
(32) Fonseca Guerra, C.; Snijders, J. G.; te Velde, G.; Baerends, E. J. *Theor. Chem. Acc.* **1998**, *99*, 391.
(33) te Velde, G.; Bickelhaupt, F. M.; van Gisbergen, S. J. A.; Fonseca Guerra, C.; Baerends, E. J.; Snijders, J. G.; Ziegler, T. *J. Comput. Chem.* **2001**, *22*, 931.
(34) Vosko, S. H.; Wilk, L.; Nusair, M. *Can. J. Phys.* **1980**, *58*, 1200.
(35) Becke, A. D. *Phys. Rev. A* **1988**, *38*, 3098.
(36) Perdew, J. P. *Phys. Rev. B* **1986**, *33*, 8822. *Phys. Rev. B* **1986**, *34*, 7406.
(37) van Lenthe, E.; Ehlers, A. E.; Baerends, E. J. *J. Chem. Phys.* **1999**, *110*, 8943.
(38) van Gisbergen, S. J. A.; Snijders, J. G.; Baerends, E. J. *Comput. Phys. Commun.* **1999**, *118*, 119.
(39) Rosa, A.; Baerends, E. J.; van Gisbergen, S. J. A.; van Lenthe, E.; Groeneveld, J. A.; Snijders, J. G. *J. Am. Chem. Soc.* **1999**, *121*, 10356.
(40) Wang, F.; Ziegler, T. *Mol. Phys.* **2004**, *102*, 2585.
(41) Wang, F.; Ziegler, T. *J. Chem. Phys.* **2004**, *121*, 12191.
(42) Wang, F.; Ziegler, T. *J. Chem. Phys.* **2005**, *122*, 074109.
(43) Gritsenko, O. V.; Schipper, P. R. T.; Baerends, E. J. *Chem. Phys. Lett.* **1999**, *302*, 199.
(44) Gross, E. K. U.; Kohn, W. *Adv. Quantum Chem.* **1990**, *21*, 255.

(45) Bolovinos, A.; Tsekeris, P.; Philis, J.; Pantos, E.; Andritsopoulos, G. *J. Mol. Spectrosc.* **1984**, *103*, 240.
(46) Schreiber, M.; Silva-Junior, M. R.; Sauer, S. P. A.; Thiel, W. *J. Chem. Phys.* **2008**, *128*, 134110.
(47) Walker, I. C.; Palmer, M. H.; Hopkirk, A. *Chem. Phys.* **1989**, *141*, 365.
(48) Tozer, D. J.; Amos, R. D.; Handy, N. C.; Roos, B. O.; Serrano-andrés, L. *Mol. Phys.* **1999**, *97*, 859.
(49) Walker, N. R.; Dobson, M.; Wright, R. R.; Barran, P. E.; Murrell, J. N.; Stace, A. J. *J. Am. Chem. Soc.* **2000**, *122*, 11138.
(50) *NIST Chemistry WebBook*. webbook.nist.gov/chemistry.